16th World Conference on Earthquake Engineering, 16WCEE 2017
Santiago Chile, January 9th to 13th 2017
Paper N° 2194
Registration Code: S-O1464715335

FORCE-BASED FINITE ELEMENT FOR MODELLING THE CYCLIC BEHAVIOUR OF UNREINFORCED MASONRY PIERS

F. Vanin[(1)], J. P. Almeida[(2)], K. Beyer[(3)]

[(1)] PhD candidate, EPFL - École Polytechnique Fédérale de Lausanne, francesco.vanin@epfl.ch
[(2)] Post-doctoral researcher, EPFL - École Polytechnique Fédérale de Lausanne, joao.almeida@epfl.ch
[(3)] Assistant professor, EPFL - École Polytechnique Fédérale de Lausanne, katrin.beyer@epfl.ch

Abstract

A performance-based seismic assessment of unreinforced masonry (URM) buildings requires the use of reliable models, able to predict their nonlinear force-displacement response including their displacement capacity. Among the possible methodologies, at different levels of complexity, macro-modelling using structural component elements has proved to be an approach that can provide satisfactory accuracy at very low computational cost, rendering it therefore suitable for engineering practice. The use of such modelling strategy requires the idealization of the structure through an equivalent frame, whose deformable elements are able to describe the in-plane response of piers or spandrels.

In this paper, the modelling of the cyclic in-plane response of a modern unreinforced brick masonry panel through a two-node, force-based beam element is proposed and validated against experimental results. The distributed inelasticity is described with the use of numerically integrated fibre sections, applying a nonlinear, biaxial material model. Such model can provide a coupling between axial and shear response at the local level, which is a novel approach for the numerical modelling of URM structural components with beam elements. The model is implemented in the open-source platform "Opensees" and is therefore available to the research community. The validation of the proposed formulation is performed through the comparison with experimental results of a shear and compression test, performed at EPFL. The experimental data, including also strain fields, allow for the comparison with numerical results both at the element level, in terms of top displacement and rotation, and at the local scale, in terms of fibre strains and sectional deformations. The comparison showed that the proposed element captures the cyclic response of unreinforced brick masonry walls in an adequate manner.

Keywords: force-based beam element, unreinforced masonry, cyclic in-plane behaviour, distributed inelasticity

1. Introduction

The assessment of the seismic behaviour of masonry buildings through refined procedures, such as static non-linear analyses or incremental dynamic analyses, requires the use of accurate and efficient numerical tools for the prediction of the structural response, in terms of strength and displacement capacity, in the monotonic and, when needed, in the cyclic range. In this context, beam models, despite the strong kinematic assumptions that they imply, still represent typically a very good compromise between accuracy of the description of the cyclic response on one side, and simplicity and computational efficiency on the other side [1–3].

Beam models of masonry walls are meant to be applied to equivalent frame modelling approaches, in which the structure is simplified into a frame of deformable elements, corresponding to piers and, when present, spandrels, connected by rigid nodes. For their characteristics, some typologies of complex buildings do not lend themselves to such a simplified structural model; however, most existing residential buildings in unreinforced masonry (URM) can be effectively modelled through this approach. Equivalent frame models are particularly suitable for modern URM buildings, presenting typically a regular layout and good connections between vertical elements and stiff horizontal diaphragms. Nonetheless, through adequate assumptions, they can be applied also to historical residential masonry buildings, provided that a box-like behaviour is ensured by the existing connections.

In equivalent frame models, damage is assumed to concentrate in the deformable beams or macro-elements, which have to give a complete description of the response of the structural element, including all the relevant non-linear phenomena and failure mechanisms that can affect it. For URM brick walls, the phenomena that influence more the response are the opening and closing of joints in flexure and the diagonal cracking of joints and eventually

units in shear. Failure mechanisms are typically classified into flexural or rocking failure, and shear failure for diagonal cracking or, less often, for sliding in the joints [4]. However, in addition to these pure modes, mixed failure mechanisms are often observed in experimental tests [5].

Equivalent frame models for URM buildings make often use of macro-elements developed to reproduce the global force-displacement response of a masonry structural element. Although they provide information only at the global level, since they are often based on simplified approaches that do not model accurately the local behaviour, macro-elements owe their large diffusion to the numerical simplicity implied in the method. A well-known macro-element was proposed by Lagomarsino et al. [6] and Penna et al. [7], which models the flexural response through two interfaces where the axial deformations are lumped, and the shear response through a damage uniaxial model. The model derives from the integration of the continuum model proposed by Gambarotta and Lagomarsino [8], and remains uncoupled from the flexural response.

A slightly more refined approach for the equivalent frame modelling of URM building is represented by beam models, in which global quantities such as nodal forces and displacements are computed together with local quantities (strains, stresses and sectional deformations), to which the limit states of the elements can be related. Among the beam element models with distributed plasticity, force-based formulations are often preferred over displacement-based elements because the force interpolation functions verify strictly equilibrium in each integration point. The sectional response is typically modelled through discretising the section into fibres. This approach is well established for reinforced concrete and steel members and can be extended to URM elements. Several authors have investigated the use of force-based beam models with fibre sections for the analysis of URM structures and these works are reviewed in the following.

Force-based beam models for modelling the response of URM walls were proposed by Roca [1] and more recently by Addessi et al. [9], resorting to simple non-linear elastic constitutive models through which the numerical integration throughout the sections can be avoided. However, these models only allow to properly simulate the monotonic behaviour of the element. As a more complex approach, applicable to the cyclic range, Raka et al. [10] recently proposed a force-based beam element with numerically integrated fibre sections for URM walls. The nonlinear behaviour in shear was tackled by a phenomenological cyclic law, uncoupled from the axial behaviour, describing the shear force-deformation relationship at the sectional level. Effects of the variable axial load on the shear capacity, and the influence of the partialisation of the section on the shear behaviour, are therefore not captured.

A proposal for a beam element coupling shear and axial behaviour directly at the fibre level is given in Ghiassi [11]. Although not formally termed as force-based beam element, the proposed approach, based on a curvature analysis and an iterative procedure to solve equilibrium at the integration section, can be considered an equivalent method to the classical formulation of a force-based beam element. The material model is a rather complex biaxial orthotropic model, using the rotating crack approach.

The present study proposes a force-based beam element for the modelling of URM walls that couples bending and shear behaviour. It is applicable to the cyclic range, opening up the possibility of conducting a large number of nonlinear time-history analyses with a limited numerical burden, which is one of the most appealing features of equivalent frame models. The axial and shear behaviour is coupled at the fibre level by means of a simple biaxial mechanical model, which is based on a Mohr-Coulomb type law. This model has been implemented by the authors in the software Opensees [12] and will be available as a free tool for the research and professional community.

This paper presents the central idea of the formulation of the material model, and compares numerical and experimental results of a wall failing in flexure. The adequateness of a beam structural model to describe the kinematics of a flexure-dominated masonry wall is discussed through the comparison with experimental deformation fields. The accuracy of the numerical model is not only checked on the global level (force-displacement response) but also on the level of local strains, and the modelling details that allow reproducing correctly the local response are briefly analysed.

2. Formulation of the beam element

The assumption of a standard Timoshenko beam model for a masonry pier implies the acceptance of the kinematic hypotheses related to the beam theory, among which the strongest and more questionable for squat masonry elements are the adoption of a continuum material model, a constant distribution of shear strains on the section and the planarity of the section in the deformed configuration. The latter condition in particular can be considered a rather crude approach; however, the strain fields measured in experimental campaigns, as will be shown, confirm that the planarity of the section may be assumed without introducing large errors, at least for walls exhibiting a flexural behaviour.

For what concerns shear deformations, after the onset of diagonal cracking in a shear wall, a non-uniform shear strain distribution is typically observed [13]. However, it is not possible to model the true nonlinearity of the shear deformation in the framework of the Timoshenko beam theory. Although alternative structural theories (higher order beam theories) can relax this latter condition assuming different deformation modes for the deformed section, in this study the classical Timoshenko beam theory is applied. One main reason is that higher order beam theories require the introduction of additional degrees of freedom at the nodes, or assumptions on deformation quantities, that render the implementation in standard finite element codes less straightforward.

If one adopts a material model that assumes that only the compressed portion of the section contributes to its shear capacity—such as the model proposed by Roca [1]— the nonlinearity in the shear response is partially captured. The shear deformations remain, however, constant along the cross section and are therefore accounted for only in an average sense.

The use of a force-based beam element is suggested by the highly nonlinear curvature profiles along the height that are obtained from experimental tests. These profiles show the development of a region where non-linear deformations concentrate [14]. In the context of distributed plasticity, these deformation profiles can be efficiently simulated by force-based beam elements, while the constraints in the deformation profile of displacement-based elements do not allow to correctly represent such concentrations of deformation, particularly when only one element is used along the height of the member.

The standard formulation of the Timoshenko force-based beam element as already implemented in Opensees [12] is adopted. Fig. 1 shows some fundamental properties of the formulation. Shape functions are used to calculate sectional forces from the nodal forces, ensuring in this way strict equilibrium at each integration section. The plane section hypothesis is used to calculate the strains (both normal and tangential components) at fibre. A nonlinear bi-dimensional material model can then link these deformations to the stresses, accounting for their interaction.

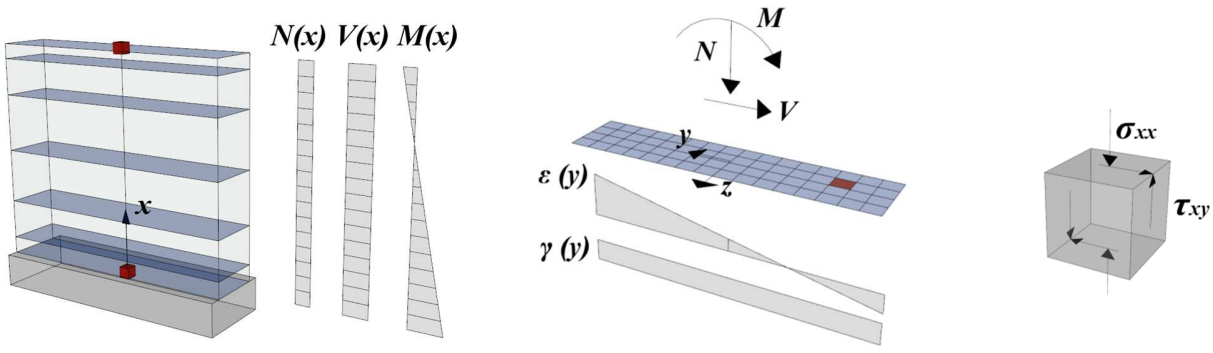

Fig. 1 – Formulation of the force-based beam element with coupling between axial and shear stress

Once the stress-strain response at the fibre level is established, numerical integration is performed along the section, and an iterative element-section state determination cycle has to be performed at each load step, rendering the solution of a force-based element less direct in comparison with a standard displacement-based element. Methods avoiding this internal iteration are available in the literature; however, they are not necessarily more

efficient. The element implemented in Opensees applies the standard method requiring an internal state-determination cycle as it has been originally proposed by Spacone et al. [15]. With regard to the original formulation, a modified version [16], using the Timoshenko beam theory to account for shear deformability, is implemented in the software.

2.1 Material model

The nonlinear response of the element originates from the nonlinearity of the material model. Such material model should describe all nonlinear phenomena triggered in in-plane loaded masonry walls, namely rocking or flexural failure and shear failure for diagonal cracking or sliding. It has further to account for their coupling. As a minimum requirement, the used material model has to be formulated in a two-component strain/stress vector, including normal and tangential stresses. If a generic two- or three-dimensional material model is adopted, some hypotheses have to be applied to the stress and/or strain components that are not considered by the beam model. The standard approach is to use a local iterative cycle which imposes that all non-modelled stress components are equal to zero.

The material model should describe complex nonlinear phenomena, such as:

- Crack opening in tension, and crack closure for reversed loading with stiffness recovery in compression, to properly model the rocking behaviour;
- Compressive failure to model toe crushing, with residual strains after damage in compression;
- Shear failure through a criterion able to take into account the influence of the axial load variation and of the decompression of part of the section under bending;
- Resistance to sliding along closed cracks, in cyclic rocking. This feature is complex to model with isotropic models that describe damage with scalar quantities independently of the direction, as the shear frictional strength would be improperly coupled with the tensile strength.

Considering these requirements, with the aim of limiting the complexity of the material model, a simple constitutive model coupling axial and shear response was formulated and implemented as a new constitutive relationship in Opensees. Fig. 2 represents the strength domain of the material model. The coupling between axial and shear stresses is ensured by the use of a Mohr-Coulomb (MC) type criterion, imposing a limit to the shear stress at each fibre depending on the current axial stress. To keep the simplicity of the formulation, the compressive failure is considered independent from the shear stresses, being the Mohr-Coulomb condition the only interaction between axial (σ) and shear (τ) stress components.

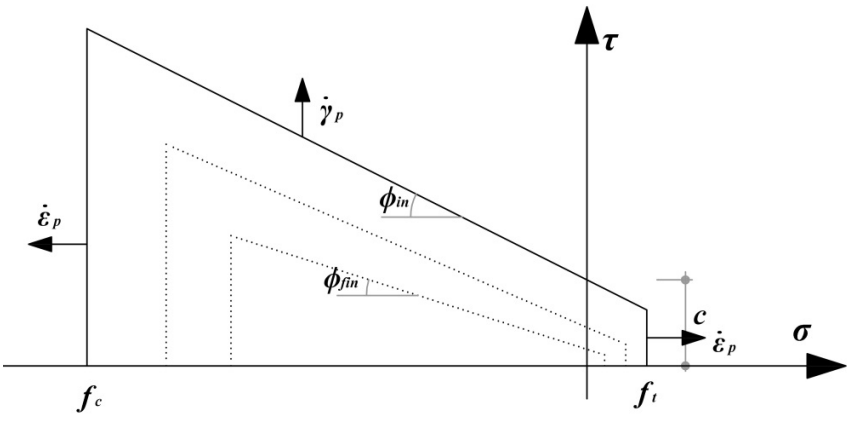

Fig. 2 – Yield domain of the material model

The basic steps in state determination of this simple biaxial material model are (1) the computation of the axial stress from the axial strain through a standard one-dimensional model, and (2) the computation of the shear stress based on the shear strain and on the updated value of axial stress, using a plastic model for shear. The material model adopted to describe the axial behaviour is the material Concrete 02, as already implemented in the source code of Opensees. This model describes compressive damage and degradation of stiffness, hysteresis in the

loading-reloading cycles, limited tensile strength, linear softening both in tension and compression, recovery of stiffness after crack closure, and a residual strength in compression.

After computing the axial stress, the Mohr-Coulomb criterion is applied to model inelasticity in the shear response. The use of a standard plasticity model implies that there is no evolution of plastic shear strains during unloading. This hypothesis is not acceptable for the axial behaviour, in which crack closure plays a fundamental role in the global response, but may be adopted for shear deformations. However, although tests of interfaces in shear show a basically elastic unloading branch and therefore confirm this hypothesis, the shear behaviour of a section after diagonal cracking is in general more complex.

The formulation of the plastic model for shear is based on the model proposed by Lourenço for interfaces [17], considering only the frictional criterion, formalised in the standard formulation of eq. 1 through the yield function f_{MC}. No dilatancy was accounted for. The cohesion c and the friction angle ϕ are expressed as function of the hardening variable κ_{MC}, whose evolution is linked to the plastic multiplier $\dot{\lambda}$ and the rate of plastic strain $\dot{\gamma}_p$ through eq. 4. The adopted hardening/softening functions are formalised in eq. 2-3, depending on one material parameter, the fracture energy G_f^{II} for mode II fracture. The degradation of the cohesion is modelled by an exponential softening law, while the initial friction angle ϕ_{in} can degrade with evolution of the plastic strain maintaining a residual strength ϕ_{fin}. The degradation of the material parameters is shown in Fig. 3.

$$f_{MC} = |\tau| + \sigma \tan\phi(\kappa_{MC}) - \overline{\sigma}_{MC}(\kappa_{MC}) \tag{1}$$

$$\overline{\sigma}_{MC} = c \exp\left(-\frac{c}{G_f^{II}}\kappa_{MC}\right) \tag{2}$$

$$\tan\phi = \tan\phi_{in} + (\tan\phi_{fin} - \tan\phi_{in})\frac{c-\overline{\sigma}_{MC}}{c} \tag{3}$$

$$\dot{\kappa}_{MC} = \dot{\lambda}, \qquad \dot{\gamma}_p = \dot{\lambda}\frac{\tau_{trial}}{|\tau_{trial}|}, \qquad \tau_{trial} = \tau_n + G\Delta\gamma_{n+1} \tag{4}$$

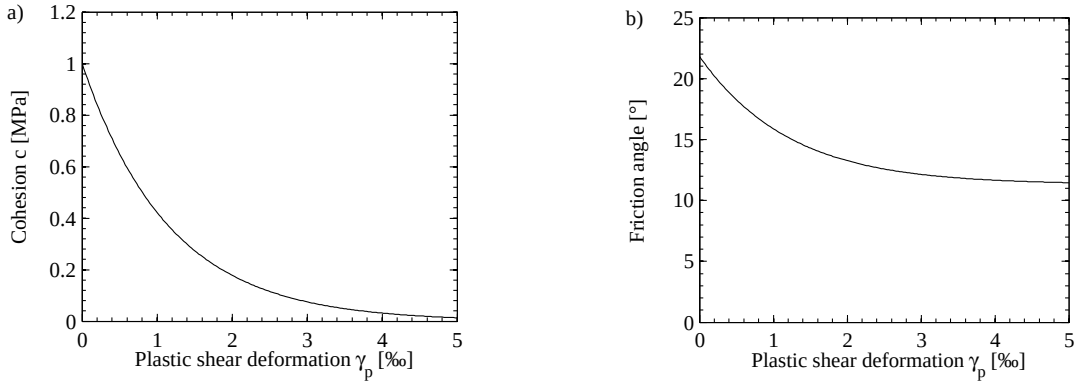

Fig. 3 – Softening laws adopted for shear failure, with degradation of the cohesion and of the friction angle (mechanical parameters: c = 1 MPa, tan ϕ_{in} = 0.4, tan ϕ_{fin} = 0.2)

For each strain increment, an implicit return mapping scheme is applied. The structure of the equations allows reducing the problem to the solution of one nonlinear equation, obtaining the increment of the plastic multiplier at step *n+1* and, from this, all the related variables. This equation is solved through a Newton-Raphson cycle at each step. Once the plastic multiplier and the stresses at the step *n+1* are determined, the algorithmic tangent matrix can be calculated from eq. 5-6 [17]. It can be noted that the adoption of a zero dilatancy angle, a choice that was aimed at decoupling the evolution of axial stress and strain from the shear criterion, led to a non-symmetric tangent stiffness matrix. This means that the flow rule, as shown in Fig. 1, is non-associated.

$$h_{MC} = \left[\sigma_{n+1}\left(\frac{\tan\phi_{fin}-\tan\phi_{in}}{c}\right)\right]\frac{\partial\overline{\sigma}_{MC}}{\partial\kappa_{MC}} \tag{5}$$

$$\boldsymbol{D}_{MC}^{ep} = \frac{\partial \boldsymbol{\sigma}}{\partial \boldsymbol{\varepsilon}}\Big|_{n+1} = \frac{1}{h_{MC}+G} \cdot \begin{bmatrix} E(\sigma) & 0 \\ -E(\sigma) \cdot G \tan\phi \frac{\tau}{|\tau|} & h_{MC} \cdot G \end{bmatrix} \quad (6)$$

Ten material parameters are required to characterise completely the response of this material: the compressive strength f_c, the initial Young's modulus, the residual strength in compression, the fracture energy in compression G_f^c, the tensile strength f_t, the fracture energy in mode I G_f^I, the initial and residual friction angles ϕ_{in} and ϕ_{fin}, the cohesion c and the fracture energy in mode II G_f^{II}. An example of the resulting cyclic behaviour at the local scale is shown in Fig. 4 for the axial and shear components.

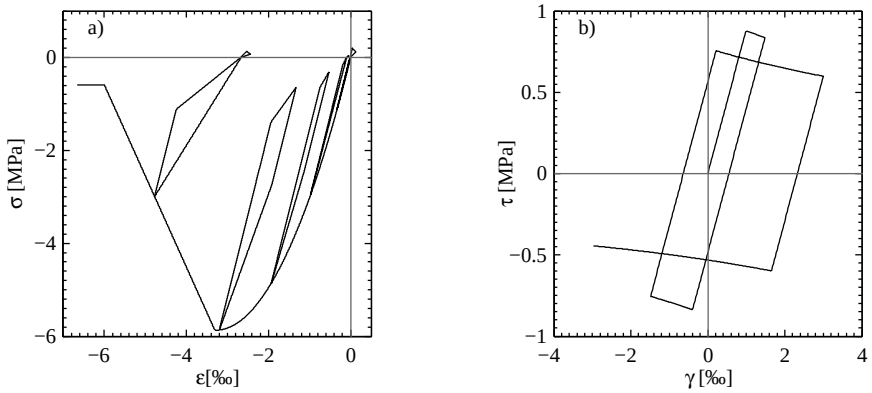

Fig. 4 – Cyclic behaviour of the material model in compression (a) and shear, under a constant axial load (b). Main material properties: f_c = 5.7 MPa, f_t = 0.25 MPa, c = 0.25 MPa, tan ϕ_{in} = 0.4, tan ϕ_{fin} = 0.2, G_f^c = 8 N/mm, G_f^I = 0.05 N/mm, G_f^{II} = 0.5 N/mm

3. Element response under different loading conditions

The behaviour of the material at the local level determines completely the cyclic response of the element. The force capacity is determined by the prevailing failure mechanism, showing a combination of flexure and shear when the two failure loads are similar. The strength domain follows the prediction of force capacity obtained through code provisions [18], obtained using the expressions given in eq. 7-9, where N is the applied axial load, L and t are, respectively, the length and the thickness of the wall, H_0 is the shear span and f_c the compressive strength. The criteria considered for shear failure are the Mohr-Coulomb criterion applied to the gross section, or on the net section. Accounting only for the partialised section to determine the shear capacity allows considering that in the cracked portion of the section the cohesive contribution is null, while the frictional contribution remains the same.

flexural force capacity: $$V_{fl} = \frac{N}{H_0} \cdot \left(\frac{L}{2} - \frac{N}{0.85 f_c\, t}\right) \quad (7)$$

shear force capacity: $$V_{MC,gross} = N \tan\phi + c\, Lt \quad (8)$$

$$V_{MC,net} = \frac{N}{2}\left[\frac{3c\, tL + 2\tan\phi\, N}{3c\, tH_0 + N}\right] \quad (9)$$

Eq. 9 is obtained expressing the length of the compressed section in the hypothesis of a linear elastic material with no tensile strength. The similarity between numerical and analytical predictions of the force capacity derives from the assumption on the local or on the sectional level, of the same failure criterion, a Mohr Coulomb law.

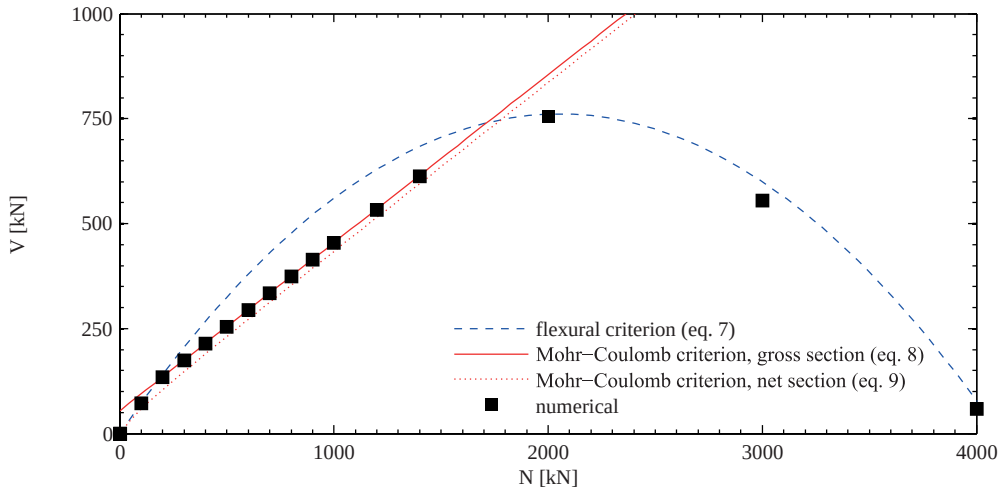

Fig. 5 – Shear force/axial force strength domain of a cantilever wall element (length 3.50 m, height 2.25 m, thickness 0.20 m; material properties as in Fig. 4)

4. Comparison with experimental results

The performance of the proposed beam element was compared to a quasi-static cyclic test on one URM wall, which was performed at EPFL [19]. The wall was built with hollow clay brick units and standard cement-based mortar. The whole test campaign consisted of six quasi-static cyclic tests on identical walls, tested under different axial load ratios and moment restraints applied at the top of the walls. The test setup, shown in Fig. 6, comprised three servo-hydraulic actuators that could be controlled in a fully-coupled mode. The two vertical actuators allowed applying an axial force and moment at the top of the wall simulating several top boundary conditions that are different from the standard cantilever and fixed-fixed configurations typically applied in shear and compression wall tests. Throughout the loading, the deformation of the walls was recorded through a digital photogrammetric measurement system, tracking the 3D position of 312 light emitting diodes (LEDs) for each test unit. The whole dataset is publically available online [19].

a) 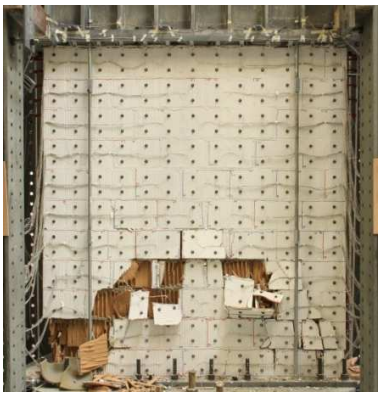 b) 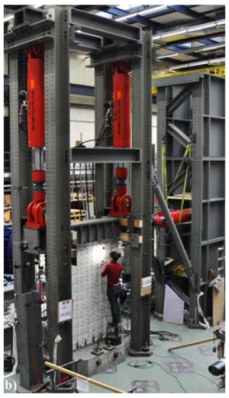

Fig. 6 –Wall PUP3 at failure (a), and test setup, showing the position of the three red actuators (b) [19]

Among the six tests, wall PUP3 was chosen for the comparison with the numerical beam model that is proposed in this paper. This test unit exhibited a flexural failure, with crushing of masonry at the toe that led the wall to losing its lateral force capacity. The dimensions of the wall are 2.25 m in height, 2.01 m in length and 0.20 m in thickness. A constant load of 419 kN was applied at the top of the wall, corresponding to an axial load ratio of 0.18. A moment was applied at the top section through the two vertical actuators, keeping a constant shear

span of 1.5H, where H is the wall height. The main mechanical parameters derived from material tests or calibrated for the numerical model are reported in Table 1. In absence of specific information on the inelastic properties in shear, and considering the flexural failure mode of the simulated wall, the shear behavior was considered elastic-plastic with no degradation of the cohesion and the friction angle.

The measurement of the LEDs' position at a frequency of 2 Hz allowed calculating the strain fields in the wall throughout the experiment. A continuous displacement field can be retrieved from the LEDs in an approach similar to the one used in the Finite Element Method, interpreting LEDs as nodes. Bilinear shape functions were used to estimate the displacement field in the area comprised between each group of four LEDs. Based on this displacement field, the strain field was computed. For the plots in Fig. 7 and Fig. 9 strains are calculated in four points for each 4-node element, in the position that would correspond to the integration points in a standard Gauss 2x2 scheme. It is known that this type of 4-node element leads to a poor estimation of the shear strain field for pure bending deformations, as it is clearly the case at the base of PUP3 wall, particularly in the cracked portion of the base section. To obtain an enhanced estimation of the strain field in bending dominated elements, a constant shear strain, calculated in the centre of the quadrilateral, is assumed for the whole element. This is an assumption that is a default option also in some finite element codes.

Table 1 – Mechanical parameters, measured in the characterisation tests or calibrated for the numerical model

measured		calibrated			
f_c	5.87 MPa	G_f^I	0.05 N/m	c	0.25 MPa
E	3550 MPa	G_f^{II}	-	$\tan\phi_{in}$,	0.4
f_t	0.25 MPa	G_f^c	8 N/m	$\tan\phi_{fin}$,	0.4

The axial strain field that is computed from the experimental results is shown in Fig. 7c. It is shown for the cycle with peak drifts of ±0.4%. The axial strain distribution is rather linear along the compressed part of horizontal sections. These strain profiles confirm the possibility to model such walls through beam models that assume that plane sections remain plane, which is a hypothesis that cannot be relaxed unless additional degrees of freedom are introduced (see Section 2). From the vertical strain profiles it is possible to obtain equivalent sectional deformations, i.e. curvatures and shear sectional deformations. To calculate these, only the compressed part of the section was taken into consideration. Linear regression of the vertical strains was used to compute the curvature, while an average of the shear strains was applied to calculate the shear deformation.

The profiles shown in Fig. 7 correspond to large drifts (0.4% and 0.8%), at which the response of the wall was already heavily nonlinear, after decompression of the base sections (Fig. 8a). At early stages, before the onset of nonlinear material response, the curvature profile showed the expected linear trend and the shear deformations were roughly constant over the height of the wall. The increase in curvature for higher drifts, as plotted in Fig. 7, applied only to the base portion of the wall, where the majority of nonlinear phenomena occur (decompression and tensile cracking of the joints, and crushing in compression in this case), while remaining linear in the rest of the element. The same consideration can be done for the shear strain profile, confirming that the decompression of part of the section affects also the shear deformation. It would be therefore desirable to take into account this interaction between flexural and shear behaviour also in the numerical model, even if the model is as simple as a beam.

These sectional deformation profiles can be reproduced with force-based elements, in which no assumption is made a-priori on the shape of the deformation profile. Much less suitable for reproducing a highly nonlinear increase of deformation are displacement-based elements, at least if only one element is used to model one wall.

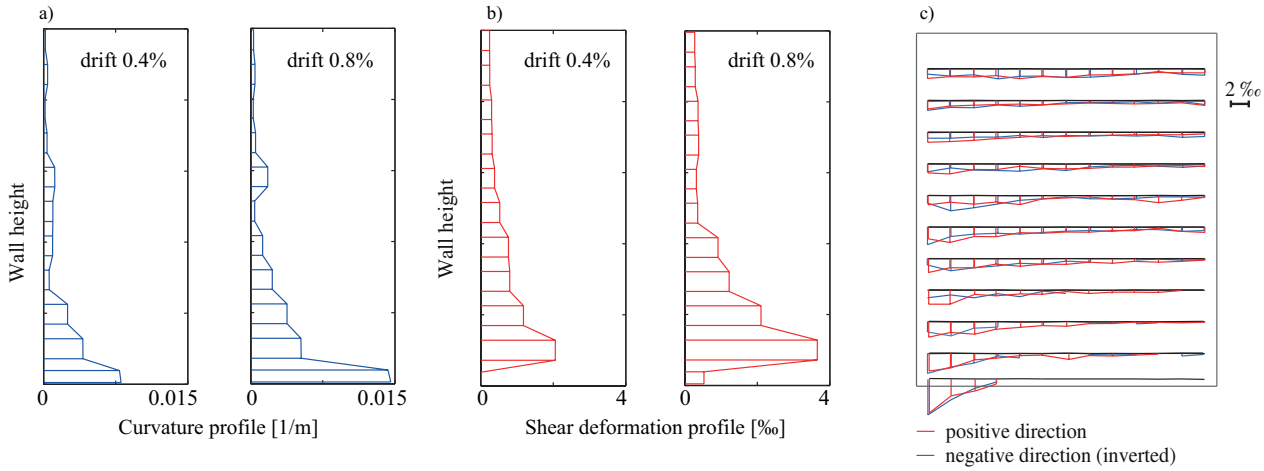

Fig. 7 – Curvature (a) and shear deformation (b) profiles at two steps of the test (drift of 0.4% and 0.8%); c) vertical strain profiles along horizontal sections at a drift of 0.4%

The failure mechanism in the tested wall consisted in the development of an inclined crack through a brick starting at the level of the first mortar joint, suggesting that compressive failure should be localised at a section at one brick height above the foundation. The lowest section showed a higher capacity in compression, probably due to the confinement effect of the concrete foundation [14]. This effect can be simulated in a beam model through introducing two integration points, chosen to match the base section and the section that actually failed. Different material properties can be attributed to the two sections, which account for the different degrees of confinement. In the model proposed here the confinement effect is not directly accounted for by the material model. Instead, increased values of compressive strength and fracture energy are assumed to simulate it indirectly; an increase of 40% of the compressive strength and the fracture energy was adopted here.

It should be noted that a change in the position of the integration points requires a recalibration of the integration weights, as standard quadrature schemes can no longer be applied. A Gauss-Lobatto scheme with seven integration points (IP) was chosen as starting point; after the adjustment of two integration points, the weights have been re-computed according to the formulation proposed by Almeida et al. [20], with the aim of optimising the accuracy of the integration scheme. A scheme with N points, in fixed positions, for which the weights of the two extreme IPs are set, integrates exactly a polynomial of order N-3, sufficient to represent the expected nonlinearity of the curvature profile.

Fig. 8 shows the comparison between the experimental global response of the wall and the numerical results, in terms of lateral force-displacement response and uplifting of the wall for rocking around the toe. The numerical and experimental curves show a fairly good match, both in the estimation of the force capacity and in the reproduction of the hysteretic behaviour. The uplifting of the wall is correctly predicted by the numerical model, as well as the stiffness degradation in the cyclic response. The model predicts that failure occurs at the second integration section, i.e. at one brick height, which agrees with the experimental observations. The sections where decompression is more relevant show also an increase of the shear deformation, although flexure remains the dominating failure mechanism.

The estimation of the displacement capacity is controlled by the choice of an appropriate value of fracture energy in compression, at least for flexural failure. Since the loss of lateral capacity is linked to a softening behaviour of the material, and consequently, of the sectional moment-curvature behaviour, localisation phenomena become relevant in determining the post-peak response and must therefore be considered [21]. The specific fracture energy, which is a material model input that determines the shape of the post-peak branch of the stress-strain relation, is expressed for a particular characteristic length. In this study a simple regularisation technique was applied, which involved a different stress-strain relation at each integration point, as a function of the ratio between the integration weight and the characteristic length, in an equivalent approach to the constant fracture energy

criterion proposed by Coleman and Spacone [22]. This approach allows avoiding completely localisation effects in the global response for uniaxial tension-compression, but is just an approximate solution for bending problems, in which not only may the displacement capacity change for different integration schemes, but also, although to a minor extent, the force capacity.

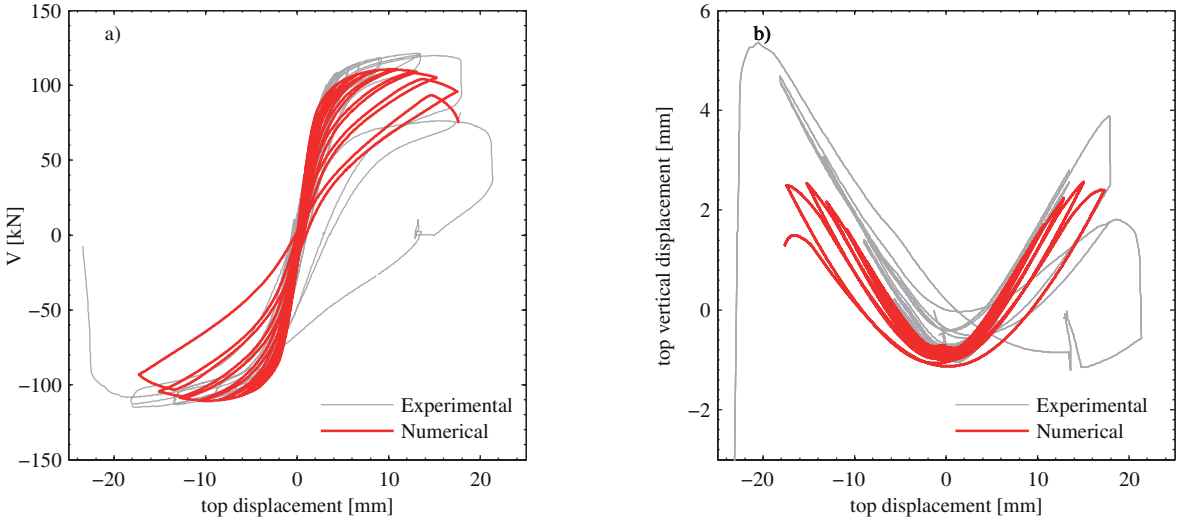

Fig. 8 – Comparison between experimental results and the global response of the beam element: a) force-displacement response and b) uplifting due to rocking followed by toe crushing failure

This method leads to minimising the non-objectiveness of the global response, but can give rather unrealistic values of local strains in the post-peak branch of the response. If it is necessary to link the limit states of the element to local measures of deformation, this feature may be problematic. The choice of a proper integration scheme, able to model correctly the experimental curvature profiles would overcome this difficulty, as wells as more advanced approaches, as the one proposed by Almeida et al. [20]. However, experimental data on deformation profiles, or good estimations of a plastic hinge length, are needed in any case, being not often available for masonry elements. In Fig. 9 the comparison between experimental and numerical results at the scale of local strains shows that such considerations, and the availability of detailed experimental data, allow for a good estimation of both the global response and the local deformation measures.

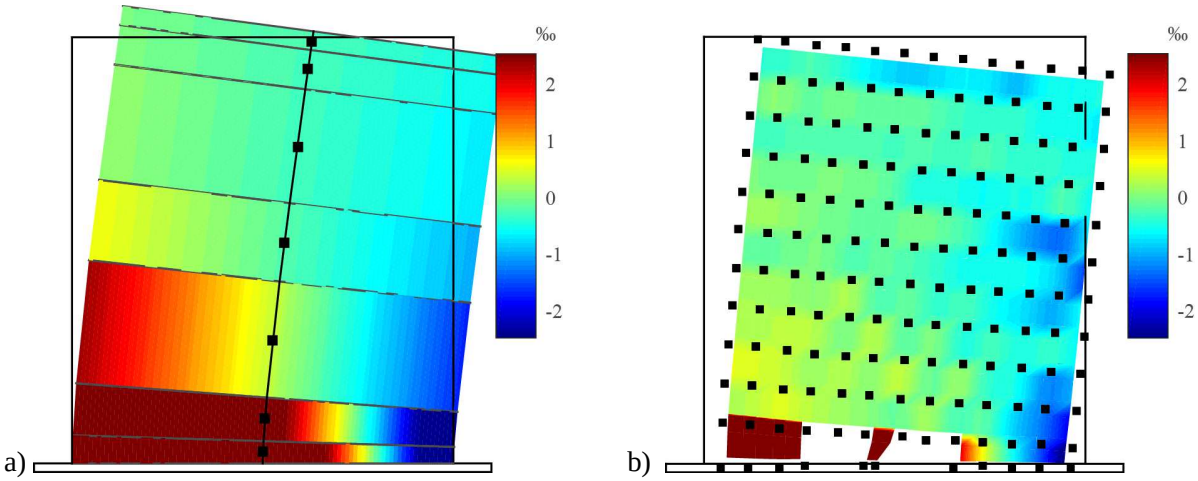

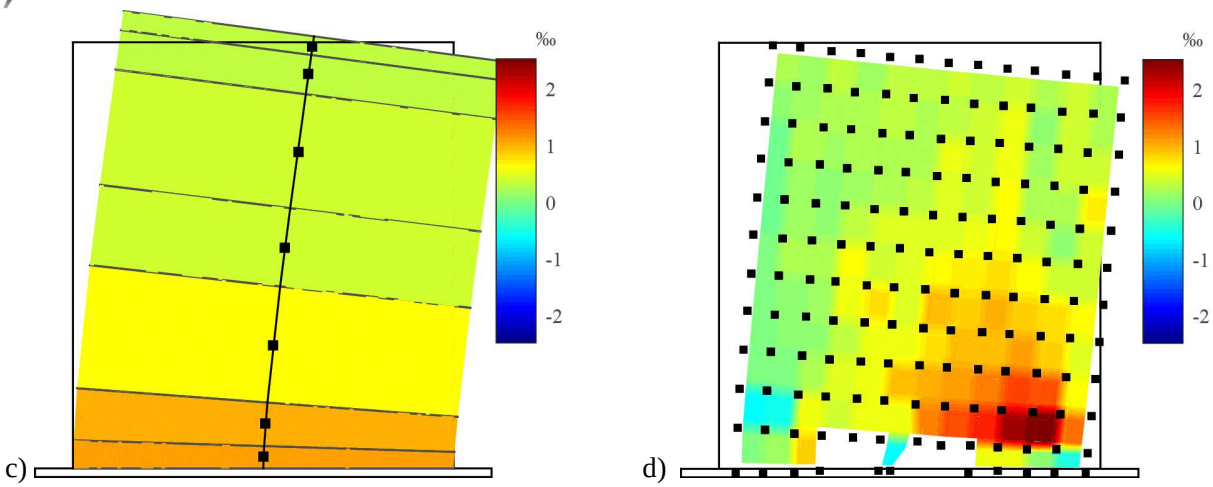

Fig. 9 – Comparison of local deformation fields. Vertical strain field of the numerical model (a) and the tested wall (b); shear strain field of the numerical model (c) and the tested wall (d)

5. Conclusions

The observation of experimental displacement and strain fields confirmed that the kinematics of a flexural dominated URM brick wall is well approximated by a beam model, and quantities such as curvatures and sectional shear strains can be derived from experimental measures. These sectional deformations show a nonlinear profile along the height that can be captured effectively by a single force-based element, while the assumptions on the deformation profiles of a single displacement-based element are not adequate to describe the experimental curvature and shear deformation profiles.

The increase of shear deformation in partially decompressed sections suggests an interaction between inelastic phenomena in flexure and shear [14], which should also be reflected in numerical models. Coupling the axial and shear response at the fibre level through 2D constitutive relationships can model directly this interaction and is able to reproduce with fairly good accuracy the experimental deformation profiles and local strains of flexural dominated URM walls, as well as the global response of the element.

When material models that include softening are used, localisation issues affect strongly the response in the post-peak branch. Adequate assumptions and modifications of standard integration schemes allow reproducing accurately local strains and deformations measured in the presented experiment, as well as the true localisation of damage. However, experimental evidence is in any case needed to justify the choice of an integration scheme or of a method to avoid localisation issues, if accurate results at local scale are needed.

Further research is needed to validate the use of beam models for unreinforced brick masonry walls showing a shear-dominated behaviour, checking the accuracy of the structural model in describing the real strain profiles and the adequateness of a material model of the type proposed in this study to capture the cyclic response of the wall. Furthermore, the comparison between numerical and experimental deformation profiles and hysteretic curves, in a consistent number of tests that develop different types of failure, can constitute a base to define reference values for the parameters of most difficult determination, such as fracture energies, as well as the most suitable integration schemes or regularisation techniques to apply. This validation procedure will allow minimising the non-objectiveness of the response and at the same time obtaining accurate local strains that could be related to the limit states of the element.

6. Acknowledgements

This project is supported by the Swiss Federal Office of the Environment and the Construction Department of the Canton Basel-Stadt.

7. References

[1] Roca, P., Molins, C. and Marí, A.R. (2005) Strength Capacity of Masonry Wall Structures by the Equivalent Frame Method. *Journal of Structural Engineering*, **131**, 1601–1610.

[2] Belmouden, Y. and Lestuzzi, P. (2009) An Equivalent Frame Model for Seismic Analysis of Masonry and Reinforced Concrete Buildings. *Construction and Building Materials*, **23**, 40–53.

[3] Penna, A., Senaldi, I., Galasco, A. and Magenes, G. (2015) Numerical Simulation Of Shaking Table Tests On Full-Scale Stone Masonry Buildings. *International Journal of Architectural Heritage*, **3058**.

[4] Magenes, G. and Calvi, G.M. (1997) In-plane Seismic Response of Brick Masonry Walls. *Earthquake Engineering & Structural Dynamics*, **26**, 1091–1112.

[5] Frumento, S., Magenes, G., Morandi, P. and Calvi, G.M. (2009) Interpretation of Experimental Shear Tests on Clay Brick Masonry Walls and Evaluation of q-factors for Seismic Design. Pavia (Italy).

[6] Lagomarsino, S., Penna, A., Galasco, A. and Cattari, S. (2013) TREMURI program: An Equivalent Frame Model for the Nonlinear Seismic Analysis of Masonry Buildings. *Engineering Structures*, **56**, 1787–1799.

[7] Penna, A., Lagomarsino, S. and Galasco, A. (2014) A Nonlinear Macroelement Model for the Seismic Analysis of Masonry Buildings. *Earthquake Engineering & Structural Dynamics*, **43**, 159-179.

[8] Gambarotta, L. and Lagomarsino, S. (1997) Damage Models for the Seismic Response of Brick Masonry Shear Walls. Part II: the Continuum Model and its Applications. *Earthquake Engineering & Structural Dynamics*, **26**, 441–462.

[9] Addessi, D., Liberatore, D. and Masiani, R. (2014) Force-Based Beam Finite Element (FE) for the Pushover Analysis of Masonry Buildings. *International Journal of Architectural Heritage*, **9**, 231–243.

[10] Raka, E., Spacone, E., Sepe, V. and Camata, G. (2015) Advanced Frame Element for the Seismic Analysis of Masonry Structures: Model Formulation and Validation. *Earthquake Engineering & Structural Dynamics*, **44**, 2489-2506.

[11] Ghiassi, B., Soltani, M. and Tasnimi, A.A. (2012) A Simplified Model for Analysis of Unreinforced Masonry Shear Walls under Combined Axial, Shear and Flexural Loading. *Engineering Structures*, **42**, 396–409.

[12] McKenna, F., Fenves, G.L., Scott, M.H. and Jeremic, B. (2000) Open System for Earthquake Engineering Simulation (OpenSees). Pacific Earthq. Eng. Res. Cent. Berkeley, California, U.S.A.

[13] Sinha, B.P., Maurenbrecher, H.P. and Hendry, A.W. (1971) Model and Full-scale Tests on a Five-Storey Cross-wall Structure Under Lateral Loading. *2nd International Brick Masonry Conference*, Stoke-on-Trent, UK.

[14] Petry, S. and Beyer, K. (2014) Limit States of Modern Unreinforced Clay Brick Masonry Walls Subjected to in-plane Loading. *Bulletin of Earthquake Engineering*, **13**, 1073–1095.

[15] Spacone, E., Filippou, F.C. and Taucer, F.F. (1996) Fibre Beam-Column Model for Non-linear Analysis of R/C Frames: Part 1. Formulation. *Earthquake Engineering & Structural Dynamics*, **25**, 711–25.

[16] Marini, A. and Spacone, E. (2006) Analysis of Reinforced Concrete Elements Including Shear Effects. *ACI Structural Journal*, **103**, 645–655.

[17] Lourenço, P.B. (1996) Computational Strategies for Masonry Structures. PhD Thesis. Delft Univesity Press.

[18] Eurocode 6. (2005) Design of Masonry Structures. Part 1-1: General rules for reinforced and unreinforced masonry structures (EN 1996-1-1).

[19] Petry, S. and Beyer, K. (2014) Cyclic Test Data of Six Unreinforced Masonry Walls with Different Boundary Conditions. *Earthquake Spectra*, **31**, 2459-2484.

[20] Almeida, J.P., Das, S. and Pinho, R. (2012) Adaptive Force-Based Frame Element for Regularized Softening Response. *Computers and Structures*, **102-103**, 1–13.

[21] Calabrese, A., Almeida, J.P. and Pinho, R. (2010) Numerical Issues in Distributed Inelasticity Modeling of RC Frame Elements for Seismic Analysis. *Journal of Earthquake Engineering*, **14**, 38–68.

[22] Coleman, J. and Spacone, E. (2001) Localization Issues in Force-Based Frame Elements. *Journal of Structural Engineering*, **127**, 1257–1265.